Applied Surface Science 55 (1992) 117–133
North-Holland

applied
surface science

Quantitative analysis of X-ray photoemission spectra, acquired on *c*-axis oriented high-T_c superconducting $YBa_2Cu_3O_{7-\delta}$ thin films

W.A.M. Aarnink, J. Gao, H. Rogalla and A. van Silfhout
University of Twente, P.O. Box 217, 7500 AE Enschede, Netherlands

Received 19 August 1991; accepted for publication 3 November 1991

Angle-resolved X-ray photoemission spectroscopy (ARXPS) was performed on *c*-axis oriented high-T_c superconducting $YBa_2Cu_3O_{7-\delta}$ thin films. The layered structure of the $YBa_2Cu_3O_{7-\delta}$ films was used to develop a model for the quantitative analysis of the ARXPS experiments. Our XPS results may be compared to spectra taken on $YBa_2Cu_3O_{7-\delta}$ single-crystal surfaces. On the spectra features are superposed that are assigned to a thin non-superconducting surface layer. For the first time, relative ARXPS measurements show that the interface between the superconducting $YBa_2Cu_3O_{7-\delta}$ film and the surface layer is formed by the atomic Y layer. The surface layer consists mainly of $BaCO_3$ and C. A small volume fraction (~ 20%) contains Ba- and Cu-oxides, probably in the form of $BaCuO_2$. From absolute ARXPS measurements, the thickness of the surface layer was calculated to be 0.93 ± 0.06 nm. It is shown that the surface roughness of our films is on the order of 0.6 nm. A good agreement between theory and experiment has been found in this report.

1. Introduction

Angle-resolved X-ray photoemission spectroscopy (ARXPS) is a widely used non-destructive tool to study the composition and thickness of the outermost top layer of solid materials (thickness ~ 6 nm) [1,2]. For the high-T_c superconducting Cu–O-based ceramics, ARXPS was used to study the spatial distribution and chemical environment of elements in the surface layer of these materials, on which many groups have reported measurements [3–15].

The basis for high-T_c superconducting devices will be formed by high-T_c superconducting multilayer structures [16–20]. The composition of interfaces in these structures plays a very important role and it strongly affects the performance of high-T_c superconducting devices. Therefore, the study of $YBa_2Cu_3O_{7-\delta}$ thin films using a surface-sensitive technique such as ARXPS is very important. It gives information about the presence, distribution and chemical environment of elements. Valuable information for the preparation of high-T_c superconducting multilayer structures or for the understanding of the behaviour of high-T_c superconducting devices may be obtained.

Until now, mainly qualitative results of ARXPS studies on $YBa_2Cu_3O_{7-\delta}$ thin films were presented in the literature. Quantitative analysis of XPS spectra is still difficult, because of the absence of adequate models. Lindberg et al. developed a model for the quantitative analysis of XPS spectra, taken on crystalline materials with a layered structure [7]. Frank et al. proposed a similar model for the quantitative analysis of XPS data, taken on $YBa_2Cu_3O_{7-\delta}$ thin films [14]. However, the first model does not include angle-resolved XPS measurements, the second model does not describe the influence of non-superconducting surface layers.

With a model we proposed earlier, we showed that ARXPS experiments enable us to determine the thickness of a surface layer with great accuracy [21]. In this report in section 2, we improve this model so that it can be used for the quantitative analysis of ARXPS spectra, taken on *c*-axis oriented high-T_c

superconducting $YBa_2Cu_3O_{7-\delta}$ thin films, covered with a non-superconducting surface layer. The layered structure of the $YBa_2Cu_3O_{7-\delta}$ thin films was used in the development of this model. To test the model, ARXPS experiments were performed on a set of $YBa_2Cu_3O_{7-\delta}$ thin films. These films were prepared in our group. After deposition, they were transported from the preparation set-up to our XPS spectrometer through ambient environment. No cleaning procedures were applied. Therefore, the $YBa_2Cu_3O_{7-\delta}$ films are covered with a non-superconducting surface layer [4–6,8,15]. (1) Application of our model for the quantitative analysis of X-ray photoemission spectra to our experimental data yields us the atomic structure of the outermost layer of the $YBa_2Cu_3O_{7-\delta}$ films; (2) the specific atomic layer at which the $YBa_2Cu_3O_{7-\delta}$ thin film changes into the non-superconducting surface layer can be determined; (3) the chemical composition of the outermost layer can be obtained; (4) a very accurate estimate of the surface layer thickness can be gained.

2. Quantitative analysis of X-ray photoemission spectra

When c-axis oriented Cu–O-based high-T_c superconducting thin films are studied with XPS, the periodic lattice of these materials must be taken into account in the analysis of the XPS spectra. Here we derive a quantitative expression for the photoemission intensity I. It describes angle-resolved experiments on materials with a layered structure parallel to the surface. It includes the effect of a non-superconducting surface layer.

For the photoelectron energy distribution $\mathrm{d}I_{i,k,p,q}(\varphi, E)$ from a core level k in atom q of element i in primitive unit cell p at depth z_p in the superconducting material (see figs. 1 and 2) we may write [1–8,21]:

$$\mathrm{d}I_{i,k,p,q}(\varphi, E) = \eta T_{\mathrm{tot}} F \Delta\Omega \gamma_{i,k} \exp\left[\frac{-(z_p + z_{i,q})}{\lambda_i \cos\varphi}\right] \exp\left(\frac{-d}{\lambda_i \cos\varphi}\right) \mathrm{d}E. \tag{1}$$

The photoelectron take-off angle is denoted by φ. The electron detector has an efficiency $\eta(E_d)$ with E_d being the kinetic energy of the photoelectrons after being transmitted through the lense and just before entering the electron detector. $T_{\mathrm{tot}}(E)$ is the total transmission of the analyser, depending on the kinetic energy E of the photoelectrons. The X-ray flux inside the sample is given by $F(x, y, \varphi)$, with the x- and y-direction parallel to the sample surface. It is assumed not to depend on the depth z in the region where the photoelectrons can escape from the material. Because of the high kinetic energy (500–1500

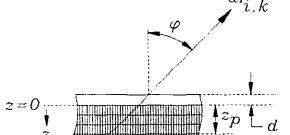

Fig. 1. Quantitative analysis of X-ray photoemission spectra. The material that is investigated, a high-T_c superconducting $YBa_2Cu_3O_{7-\delta}$ thin film, has a layered structure parallel to the surface. The effect of a non-superconducting surface layer on the photoelectron intensity is described by a transmission factor, see section 2.

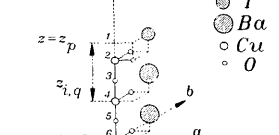

Fig. 2. Possible primitive unit cell of the orthorhombic phase of $YBa_2Cu_3O_{7-\delta}$ (schematic). Layer 1 is the Y layer, layer 2 the CuO_2 layer, layer 3 the BaO layer, etc. See sections 2 and 4.2.

eV), interactions between photons and the sample surface are neglected [22]. With a small acceptance angle of the photoelectron analyser, denoted by $\Delta\Omega$, elastic scattering of photoelectrons during transport through the solid is negligible [23]. In our experimental set-up, described in section 3, diffraction of X-rays at the sample surface can be neglected [24]. The probability of an electron to absorb an X-ray dose and being ejected from orbital k in element i with an kinetic energy $(E, \mathrm{d}E)$, is given by $\gamma_{i,k}(\vartheta_k, E)$, the angular differential photoionization cross-section [25,26]. ϑ_k is the angle between X-ray photon and photoelectron path. The inelastic mean free path (IMFP) of the photoelectrons inside the material is given by $\lambda_i(E)$ [27]. The superconducting material may be covered with a non-superconducting surface layer with thickness d, as in the case of c-axis oriented high-T_c superconducting $YBa_2Cu_3O_{7-\delta}$ thin films. This surface layer differs in chemical composition or structure. A term describing the transmission of the photoelectrons through this layer is included in eq. (1).

To obtain the total photoelectron energy distribution $\mathrm{d}I_{i,k}(\varphi, E)$ from a core level k in an atom of element i, first eq. (1) is summed over one primitive unit cell and, subsequently, summed over all primitive unit cells in the lattice:

$$\mathrm{d}I_{i,k}(\varphi, E) = \eta\Delta\Omega\gamma_{i,k} \exp\left(\frac{-d}{\lambda_i \cos\varphi}\right) K(\varphi, E)\, \mathrm{d}E, \tag{2}$$

$$K(\varphi, E) = \sum_{\text{unit cell}} \exp\left[\frac{-z_{i,q}}{\lambda_i \cos\varphi}\right] \sum_{\text{lattice}} T_{\text{tot}} F \exp\left[\frac{-z_p}{\lambda_i \cos\varphi}\right]. \tag{3}$$

Effects of imperfections in the crystal structure are neglected. Introduction of a fraction f_i of sites occupied by an atom of element i may describe the effect of imperfections. Comparison of the experimental and theoretical values will indicate if the introduction of the fraction f_i is needed.

In $K(\varphi, E)$, the summation over the whole lattice is performed in the x-, y-, and z-direction, with the x- and y-direction in the plane of the sample surface. The X-ray flux F and transmission T_{tot} do not depend on depth z in the region where the photoelectrons escape. The second summation in $K(\varphi, E)$ in eq. (3) may be written as a product of a summation of $T_{\text{tot}} \times F$ (in the x- and y-direction) and a summation of $\exp(-z_p/\lambda_i \cos\varphi)$ (in the z-direction). The summation of $T_{\text{tot}} \times F$ may be rewritten as an integral over the analysis area $A_a(\varphi)$, depending on photoelectron take-off angle φ. T_{tot} may be assumed to depend only on kinetic energy E of the photoelectrons inside the analysis area and to equal 0 outside A_a. Since F may vary over the analysis area, we define a mean X-ray flux $\overline{F(\varphi)}$. With these definitions, we may rewrite eq. (3):

$$K(\varphi, E) = T_{\text{tot}}(E)\,\overline{F(\varphi)}\,A_a(\varphi) \sum_{\text{unit cell}} \exp\left[\frac{-z_{i,q}}{\lambda_i \cos\varphi}\right] \sum_{z_i} \exp\left[\frac{-z_p}{\lambda_i \cos\varphi}\right]. \tag{4}$$

Defining a structural factor $S_i(\varphi)$ and geometrical factor $g_i(\varphi)$, respectively:

$$S_i(\varphi) = \sum_{\text{unit cell}} \exp\left[\frac{-z_{i,q}}{\lambda_i \cos\varphi}\right], \quad g_i(\varphi) = \sum_{z_i} \exp\left[\frac{-z_p}{\lambda_i \cos\varphi}\right] = \left[1 - \exp\left(\frac{-c}{\lambda_i \cos\varphi}\right)\right]^{-1}, \tag{5}$$

with c being the lattice constant in the c-direction, we obtain:

$$\mathrm{d}I_{i,k}(\varphi, E) = \eta\, T_{\text{tot}}(E)\,\overline{F(\varphi)}\,A_a(\varphi)\Delta\Omega\gamma_{i,k} \exp\left(\frac{-d}{\lambda_i \cos\varphi}\right) S_i(\varphi) g_i(\varphi)\, \mathrm{d}E. \tag{6}$$

With the result the photoemission intensity $I_{i,k}(\varphi)$ may be written as:

$$I_{i,k}(\varphi) = \eta\, T_{\text{tot}}(E)\,\overline{F(\varphi)}\,A_a(\varphi)\Delta\Omega \times \sigma_{i,k} \frac{1}{4\pi}\left[1 - \tfrac{1}{4}\beta_{i,k}(3\cos^2\vartheta_k - 1)\right] \exp\left(\frac{-d}{\lambda_i \cos\varphi}\right) S_i(\varphi) g_i(\varphi), \tag{7}$$

with $\sigma_{i,k}$ being the photoionization cross-section [25] and $\beta_{i,k}$ the asymmetry factor [26].

Eq. (7) describes the absolute photoelectron intensity when a material with a layered structure parallel to the surface is studied by ARXPS. In eq. (7), effects of imperfections in the crystal structure has been neglected. Possible reconstruction or relaxation in the high-T_c superconducting thin film just below the surface layer has been neglected. Also effects of surface roughness have not been included. In the model, the effect of a surface layer on the photoelectron intensity is described by a transmission factor $\exp(-d/\lambda \cos\varphi)$. The surface layer may be treated in the same way as the layered material beneath it by describing it by a structural and geometrical factor. For the material we investigated, thin films of high-T_c superconducting $YBa_2Cu_3O_{7-\delta}$, the structure is well known. In contrast to this, the structure of the surface layer on high-T_c superconducting $YBa_2Cu_3O_{7-\delta}$ thin films is not known well. It may consist of $BaCuO_2$, but possibly its structure has changed due to reconstruction or relaxation. Therefore, no attempt was made to model the surface layer by a structural and geometrical factor.

2.1. Relative ARXPS measurements

For the photoelectron intensity $R_{i,j}(\varphi)$ ratio of element i and j in the superconducting material below a non-superconducting surface layer, used in relative ARXPS measurements, we may write using eq. (7):

$$R_{i,j}(\varphi) = \frac{\sigma_{i,k}\left[1 - \frac{1}{4}\beta_{i,k}(3\cos^2\vartheta_k - 1)\right] T_{tot}(E_i) \exp\left(\frac{-d}{\lambda_i \cos\varphi}\right) S_i(\varphi) g_i(\varphi)}{\sigma_{j,l}\left[1 - \frac{1}{4}\beta_{j,l}(3\cos^2\vartheta_k - 1)\right] T_{tot}(E_j) \exp\left(\frac{-d}{\lambda_j \cos\varphi}\right) S_j(\varphi) g_j(\varphi)}. \tag{8}$$

Using this equation, we can compare the measured relative intensities $R_{i,j}(\varphi)$ with the ratio of the structural factors $S_i(\varphi)$ and $S_j(\varphi)$, obtained from theory by defining:

$$X_{i,j}^{exp}(\varphi) = R_{i,j}(\varphi) \frac{\sigma_{j,l}\left[1 - \frac{1}{4}\beta_{j,l}(3\cos^2\vartheta_k - 1)\right] T_{tot}(E_j) \exp\left(\frac{-d}{\lambda_j \cos\varphi}\right) g_j(\varphi)}{\sigma_{i,k}\left[1 - \frac{1}{4}\beta_{i,k}(3\cos^2\vartheta_k - 1)\right] T_{tot}(E_i) \exp\left(\frac{-d}{\lambda_i \cos\varphi}\right) g_i(\varphi)} = \frac{S_i(\varphi)}{S_j(\varphi)}. \tag{9}$$

Since the structural factors depend strongly on the choice of the primitive unit cell, we can determine the primitive unit cell that describes relative ARXPS measurements optimally. This yields us the plane at which the c-axis oriented high-T_c superconducting $YBa_2Cu_3O_{7-\delta}$ thin film starts below a non-superconducting surface layer. Also a good estimate for the thickness d of the surface layer can be found.

2.2. Absolute ARXPS measurements

With absolute ARXPS measurements, the normalized photoelectron intensity (or angle-resolved signal ratio (ARSR) [36]) $N_{i,k}(\varphi)$ is used. $N_{i,k}(\varphi)$ equals the ratio of the intensity $I_{i,k}(\varphi)$ detected at photoelectron take-off angle φ and the intensity $I_{i,k}(0)$ detected at normal take-off. With eq. (7), $N_{i,k}(\varphi)$ may be written as:

$$N_{i,k}(\varphi) = \frac{\exp\left(\frac{-d}{\lambda_i \cos\varphi}\right)}{\exp\left(\frac{-d}{\lambda_i}\right)} \frac{\overline{F(\varphi)} A_a(\varphi)}{\overline{F(0)} A_a(0)} \frac{S_i(\varphi) g_i(\varphi)}{S_i(0) g_i(0)}. \tag{10}$$

If $N_{i,k}(\varphi)$ is measured on an amorphized Si sample, cleaned by Ar ion beam sputtering, we may write:

$$S_{Si} = \int_z n_{Si} \exp\left(\frac{z}{\lambda_{Si} \cos \varphi}\right) dz, \quad g_{Si} = 1, \tag{11}$$

with n_{Si} the atomic Si concentration. If the Si 2p core level is measured, eq. (10) becomes (see also ref. [21]):

$$N_{Si,2p}(\varphi) = \frac{\overline{F(\varphi)} A(\varphi)}{\overline{F(0)} A(0)} \cos \varphi = G(\varphi). \tag{12}$$

This function $G(\varphi)$ depends on the geometry of the experimental set-up, sample and sample holder and can be measured directly. Its value can be used in eq. (10).

We may write by using eqs. (10) and (12) for the normalized intensity of e.g. the Ba 4d XPS peak of Ba in a high-T_c superconducting $YBa_2Cu_3O_{7-\delta}$ thin film below the surface layer:

$$N_{Ba,4d}(\varphi) = \frac{I_{Ba,4d}(\varphi)}{I_{Ba,4d}(0)} = \exp\left[\frac{d}{\lambda_{Ba,4d}}\left(1 - \frac{1}{\cos \varphi}\right)\right] \frac{G(\varphi)}{\cos \varphi} \frac{S_{Ba}(\varphi) g_{Ba}(\varphi)}{S_{Ba}(0) g_{Ba}(0)}. \tag{13}$$

Defining:

$$Y^{exp}_{Ba,4d}(\varphi) = \frac{\cos \varphi \, S_{Ba}(0) g_{Ba}(0)}{G(\varphi) S_{Ba}(\varphi) g_{Ba}(\varphi)} N_{Ba,4d}(\varphi) = \exp\left[\frac{d}{\lambda_{Ba,4d}}\left(1 - \frac{1}{\cos \varphi}\right)\right] \tag{14}$$

gives us an additional possibility to calculate the thickness d of the surface layer on top of the c-axis oriented high-T_c superconducting $YBa_2Cu_3O_{7-\delta}$ thin film, after having determined the structural factors that describe relative ARXPS measurements optimally, see section 2.1. In deriving eq. (14), we assumed that the surface layer has a uniform thickness d. Effects of surface roughness have been neglected.

2.3. Data analysis by a modified Levenberg–Marquardt (LM) method

Eq. (14), describing absolute ARXPS measurements on high-T_c superconducting $YBa_2Cu_3O_{7-\delta}$ thin films, contains only one parameter, the thickness d of the non-superconducting surface layer. This parameter can be optimized by minimizing the error function F:

$$F = \sum_i (Y_i - Y_i^{exp})^2, \tag{15}$$

where Y_i is the value of quantity Y predicted by theory and Y_i^{exp} is the measured value. The minimization is performed by a modified Levenberg–Marquardt method which yields the optimized parameters [28]. Also the residue s, defined as [29]:

$$s = F/(K - 1 - p), \tag{16}$$

where K is the number of measurements and p the number of parameters in the model, can be calculated. Confidence limits of the parameters can be obtained using the variance–covariance matrix. In combination with the residue s they provide a good check for the quality of the fit [29].

3. Experimental

The high-T_c superconducting $YBa_2Cu_3O_{7-\delta}$ thin films have been deposited by a modified off-axis RF-magnetron sputtering technique. Experimental details can be found elsewhere [16,17]. As substrates yttria-stabilized ZrO_2 (YSZ) (100) single crystals were used.

After deposition of the $YBa_2Cu_3O_{7-\delta}$ thin films, the samples were transported through ambient environment to the XPS instrument, a Kratos XSAM 800 spectrometer, controlled by a PDP 11 minicomputer. The samples and a copper foil, used for calibration of the spectrometer, were mounted on a carousel in the preparation chamber. After closing the introduction valve, the chamber was pumped for 14 h. The chamber walls were heated up to approximately 70°C and the pressure in the preparation chamber decreased to 1×10^{-9} Torr. After opening the valve to the analysis chamber, the carousel was introduced and the valve was closed again.

During analysis, the photoelectron energy analyser angle was fixed at 9° (high magnification) [30]. The analyser mode and resolution were set to fixed analyser transmission (FAT) and medium (ME), respectively, so the resolution of the analyser does not depend on the kinetic energy E of the photoelectrons. The transmission T_{tot} of the analyser is proportional to E^{-1} [30]. The spectrometer was calibrated by measuring the Cu $2p_{3/2}$ XPS peak and the X-ray-induced Cu L_3MM Auger peak on a clean, argon ion beam sputtered copper foil using a Mg anode [31]. Its linearity was checked [30]. The Mg Kα X-ray source was typically operated at an anode voltage of 15 kV and an emission current of 15 mA. During measurements, the pressure in the analysis chamber was typically 4×10^{-10} Torr. In the experimental set-up, the angle between X-ray photon and photoelectron path is 70°.

The spectra were taken using the DS800 program [32]. Except for the photoelectron take-off angle, all the measurements were done with the same instrumental settings. The high-T_c superconducting $YBa_2Cu_3O_{7-\delta}$ thin films were mounted using a Ta mask. Therefore, the samples were well grounded and no corrections of the photoemission spectra for charging effects were necessary. Care was taken that the mask did not partly cover the analysis area of the photoelectron energy analyser. This was confirmed by inspecting the photoemission spectra for Ta peaks, which could not be observed. The spectra of different elements were taken simultaneously by repeatedly scanning the different core levels, to minimize the influence of time-dependent effects such as fluctuations in the X-ray source intensity. The background subtraction, simulations and data analysis were done on a 80386/80387 personal computer. For background subtraction, we used the method of Shirley [33]. In all simulations of photoemission spectra, 100% Gaussians were used.

4. Results

By means of the modified RF-magnetron sputtering technique, as mentioned in section 3, high-T_c superconducting $YBa_2Cu_3O_{7-\delta}$ thin films with a transition temperature $T_{c,zero}$ of about 90 K were obtained routinely for film thicknesses of 8–300 nm. The critical current density j_c at 77 K of these films is found to be higher than 1×10^6 A/cm^2. With X-ray diffraction analysis, besides the substrate reflections only the (00l) reflections could be observed [16–20].

In this report XPS spectra are given that were acquired on a typical high-T_c superconducting $YBa_2Cu_3O_{7-\delta}$ thin film on a YSZ (100) single crystal. The spectra were measured on the sample as received. Between deposition of the $YBa_2Cu_3O_{7-\delta}$ thin film and analysis in the XPS spectrometer no cleaning procedures were applied. The film had a thickness of 10 nm, its $T_{c,zero}$ was 88 K. In studying films with comparable thicknesses on $SrTiO_3$ and MgO (100) single crystals, no essential differences in the spectra shown here were observed.

4.1. Photoemission spectra, acquired on a high-T_c superconducting $YBa_2Cu_3O_{7-\delta}$ thin film

For the elements Y, Ba, Cu, O and C, ARXPS core level spectra were recorded at photoelectron take-off angles of 0°, 10°, ..., 70°, to obtain information about the distribution and chemical environment of these elements. For the elements the spectra measured at take-off angles of 0° and 60° are shown in

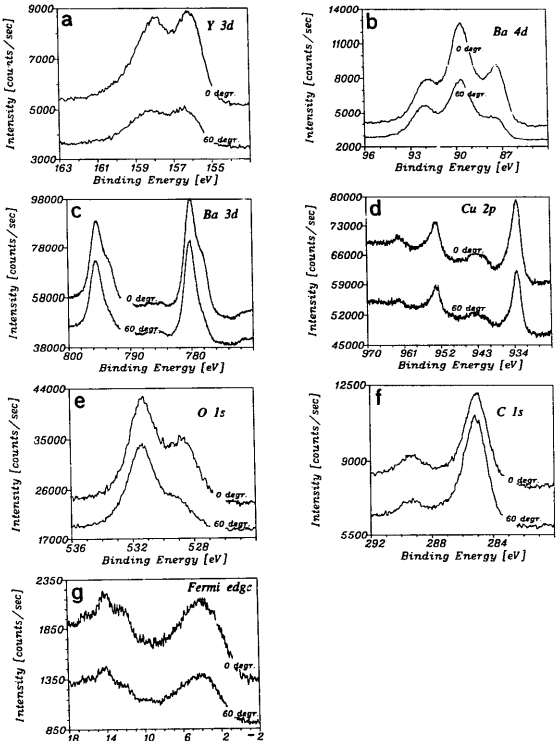

Fig. 3. X-ray photoemission spectra, acquired on a high-T_c superconducting $YBa_2Cu_3O_{7-\delta}$ thin film as received. The photoelectron take-off angles equaled 0° and 60°. A MgKα anode was used as X-ray source. Shown are: (a) the Y 3d, (b) the Ba 4d, (c) the Ba 3d, (d) the Cu 2p, (e) the O 1s and (f) the C 1s core level spectra. In (g) the Fermi edge spectrum is shown. See section 4.1.

figs. 3a–3g. It should be noted that these spectra are presented as they were obtained. No corrections for charging effects were needed, see section 3. No smoothing procedures had to be used.

In the Y 3d spectrum, shown in fig. 3a, no chemical shift can be observed. The shape of the spectrum does not change with photoelectron take-off angle. It resembles the spectrum of Y, present in one

Table 1
Binding energies and assignment of the features in the core level photoemission spectra, acquired on a high-T_c superconducting $YBa_2Cu_3O_{7-\delta}$ thin film as received (see section 4.1 and fig. 3)

Core level	Binding energy (eV)	Assignment
Y 3d	156.2	Y in superconducting $YBa_2Cu_3O_{7-\delta}$
Ba $5p_{5/2}$	12.5	
	14.0	
Ba $4d_{5/2}$	87.3	
	89.3	Low BE component: Ba in superconducting $YBa_2Cu_3O_{7-\delta}$
Ba $3d_{5/2}$	777.9	High Be component: Ba in surface layer
	780.0	
Ba $3d_{3/2}$	793.1	
	795.3	
O 1s	528.6	O in superconducting $YBa_2Cu_3O_{7-\delta}$
	531.3	O in surface layer
Cu 2p	933.1	Cu in superconducting $YBa_2Cu_3O_{7-\delta}$ and in surface layer
	~ 943	Satellite of Cu in superconducting $YBa_2Cu_3O_{7-\delta}$
C 1s	285.0	C in surface layer
	289.5	C in $BaCO_3$ in surface layer

chemical environment only. For the Y $3d_{5/2}$ core level, a binding energy of 156.2 eV was found (see table 1). This is indicative for Y in the superconducting $YBa_2Cu_3O_{7-\delta}$ thin film [3,5,6,9–11].

Contrary to the Y 3d spectrum, the Ba 4d and Ba 3d spectra, shown in figs. 3b and 3c respectively, show a clear chemical shift and contributions of Ba in two different chemical states can clearly be seen. The intensity of the high BE component increases when compared to the low BE component with increasing photoelectron take-off angle. So the low BE component can be attributed to Ba in the superconducting $YBa_2Cu_3O_{7-\delta}$ and the high BE component to Ba in a non-superconducting surface layer [3,5,6,9–11]. The BE values can be found in table 1.

The X-ray photoemission spectrum of the Cu $2p_{3/2}$ level is shown in fig. 3d. The ratio of the intensity I_{sat} of the satellite near 943 eV and the intensity I_{main} of the mean feature at 933.1 eV decreases from 0.31 to 0.18 when the photoelectron take-off angle is increased from 0° to 60°. This means that the satellite originates from Cu atoms in the superconducting material. The main feature contains contributions of both, Cu in the superconducting $YBa_2Cu_3O_{7-\delta}$ film and the non-superconducting surface layer. Steiner et al. reported X-ray photoemission spectra of Cu–O systems where the Cu has a valence of 0, +1, +2 and +3 [34]. Since Cu^{2+} has a very strong satellite near 943 eV as compared to Cu^{1+} and Cu^{3+}, we may conclude that in the superconducting material the Cu has a valence of +2. From the BE at which the main feature is found, we find that the valence of Cu in the surface layer equals +1, a result that agrees with the literature [3,9,11–13], see also table 1. The valence of Cu found in the surface layer strongly suggests that this Cu is in the form of $BaCuO_2$ [6].

In the O 1s spectrum, shown in fig. 3e, we observe as in the case of Ba, features of O in two different chemical states. From their photoelectron take-off angle dependence, the low BE component at 528.6 eV can be assigned to O in the superconducting material and the high BE component at 531.3 eV to O in the surface layer, see also table 1 [3,5,6,9–11].

In fig. 3f the C 1s spectrum is given. Clearly contributions of graphite and some $BaCO_3$ near 285.0 and 289.5 eV, respectively, can be observed. The intensity of the peak attributed to $BaCO_3$ decreases when compared to the intensity of the graphite peak under glancing incidence. This indicates that this $BaCO_3$

is covered by graphite. The carbon contaminations detected here are expected to be due to the transport of the film through ambient environment from deposition to the XPS analysis set-up.

In fig. 3g the Fermi edge spectrum, measured at 0° and 60° photoelectron take-off angle, is presented. The structure at 11–18 eV can be attributed to the Ba 5p levels. As in the case of the Ba 4d spectrum, a clear chemical shift can be observed and the low BE feature near 12.5 eV can be assigned to the Ba $5p_{5/2}$ level of Ba in the superconducting $YBa_2Cu_3O_{7-\delta}$ thin film. The high BE feature near 14 eV is ascribed partly to Ba $5p_{5/2}$ in the surface layer and partly to Ba $5p_{3/2}$ in the superconducting material (compare the Ba 4d level) [3,9,12]. Also in this case, the low BE component decreases in intensity with increasing photoelectron take-off angle. The feature near 10 eV is ascribed to a "satellite", with a Cu d^8 final-state character. The broad feature at 6–8 eV is assigned to O 2p states [9,12,13].

4.2. The interface between the superconducting $YBa_2Cu_3O_{7-\delta}$ thin film and the non-superconducting surface layer

In relative ARXPS measurements the photoelectron intensity ratio $R_{i,j}$ is used, as defined in eq. (4). To determine the intensities I_i's of elements in the superconducting material, from the spectra first a Shirley-type background [33] was subtracted. The spectra were simulated using 100% Gaussians. The intensities I_i's of the elements in the superconducting $YBa_2Cu_3O_{7-\delta}$ below the non-superconducting surface layer then equal the area below the Gaussians. The assignment is outlined in section 4.1, see also table 1.

In figs. 4a–4d the simulations of the spectra of the Y 3d, Ba 4d, Ba $3d_{5/2}$ and O 1s core level spectra are presented. The spectrum of Y 3d, measured at 0° and 60° take-off angle (see fig. 4a), can be simulated with two Gaussians representing the Y $3d_{5/2}$ and Y $3d_{3/2}$ components of Y in the superconducting $YBa_2Cu_3O_{7-\delta}$ thin film, respectively. The intensity ratio between the Y $3d_{5/2}$ and Y $3d_{3/2}$ orbitals was 1.15 and the binding energy difference equaled 2.00 eV. The somewhat high BE tail will be discussed in section 5. The Ba 4d spectrum, shown in fig. 4b, has been simulated with two sets of two Gaussians where the two Gaussians represent the Ba $4d_{5/2}$ and Ba $4d_{3/2}$ orbitals, respectively. The intensity ratio of the Ba $4d_{5/2}$ and Ba $4d_{3/2}$ orbitals equaled 1.43, whereas the binding energy difference was 2.58 eV. The low BE Gaussians set is assigned to Ba in the superconducting film, the high BE components to Ba in the surface layer. In fig. 4c the Ba $3d_{5/2}$ core level spectrum has been simulated with two Gaussians. The low BE Gaussian represents the Ba $3d_{5/2}$ level in the superconducting $YBa_2Co_3O_{7-\delta}$ and the high BE Gaussian is assigned to Ba in the surface layer. The Ba $3d_{3/2}$ level has also been simulated. Because the results are similar except for the BE's (see table 1), they are not shown here. For O 1s, the simulations can be found in fig. 4d. Also in this case, the low BE Gaussian represents the O 1s level in the $YBa_2Cu_3O_{7-\delta}$, the high BE Gaussian the O 1s level in the surface layer. For Cu no simulations were performed. As outlined in section 4.1, the intensity I_{sat} of the satellite near 943 eV is a measure for the Cu $2p_{3/2}$ intensity $I_{Cu\,2p_{3/2}}$ of Cu in the $YBa_2Cu_3O_{7-\delta}$. For the ratio $I_{sat}/I_{Cu\,2p_{3/2}}$, in the literature a value of 0.55 can be found for $YBa_2Cu_3O_{7-\delta}$ [12,13]. From I_{sat} the intensity $I_{Cu\,2p_{3/2}}$ of Cu in the superconducting $YBa_2Cu_3O_{7-\delta}$ can be calculated.

As defined in eq. (8), the relative photoelectron intensities $R_{i,j}(\varphi)$ also depend on the photoionization cross-section $\sigma_{i,k}$, the asymmetry factor $\beta_{i,k}$, the transmission $T_{tot}(E_i)$ of the analyser, the thickness d of the surface layer and the geometrical factor $g_i(\varphi)$ and the structural factor $S_i(\varphi)$. The values of $\sigma_{i,k}$ and $\beta_{i,k}$ can be found in the literature [25,26] and are listed in table 2. The angle between X-ray photon and photoelectron path equals 70° (see also section 3). For the inelastic mean free paths (IMFP's) $\lambda(E)$ of the photoelectrons, the values as shown in table 2 were taken [27]. The transmission $T_{tot}(E)$ of the analyser is proportional to E^{-1} [30], with E the kinetic energy of the photoelectrons. The kinetic energies of the photoelectrons (a Mg Kα X-ray source was used) and the values of T_{tot}, relative to $T_{tot}(E_{O\,1s})$ are listed in table 2. The geometrical factors $g_i(\varphi)$, as defined in eq. (5) and calculated at 0°

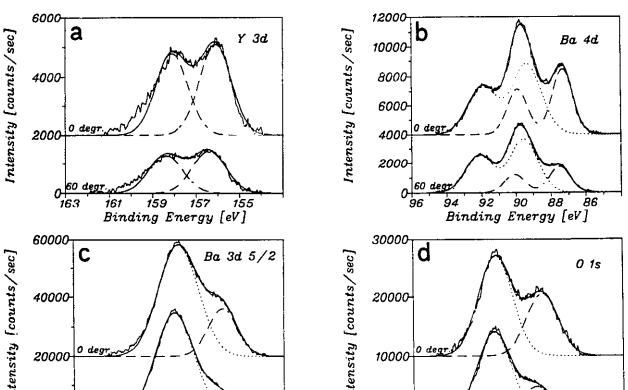

Fig. 4. Simulations of (a) the Y 3d, (b) the Ba 4d, (c) the Ba $3d_{5/2}$ and (d) the O 1s core level spectra. A Shirley-type background was subtracted prior to simulation. 100% Gaussians were used. The dashed Gaussians represent contributions of elements in the superconducting $YBa_2Cu_3O_{7-\delta}$ material, the dotted Gaussians are ascribed to elemental contributions of a non-superconducting surface layer, see section 4.2. The BE's are given in table 1. For easy comparison the spectra recorded at 0° photoelectron take-off angle have been given an offset.

and 60° take-off angle, can also be found in table 2. For the lattice constant c in the c-direction 1.168 nm was chosen [35].

The structural factor $S_i(\varphi)$ depends strongly on the choice of the primitive unit cell and, therefore, on the choice of the plane at which the high-T_c superconducting $YBa_2Cu_3O_{7-\delta}$ thin film electronically

Table 2
Relative ARXPS measurements – the Y layer forms the interface between the superconducting $YBa_2Cu_3O_{7-\delta}$ thin film and the non-superconducting surface layer (see fig. 2, sections 2 and 4.2)

XPS peak	σ [σ_{C1s}]	β	λ (nm)	E_{kin} (eV)	T_{tot}	$\varphi = 0°$		$\varphi = 60°$		$\varphi = 0°$		$\varphi = 60°$	
						$g_i(0)$	$S_i(0)$	$g_i(60)$	$S_i(60)$	$X_{i,O1s}^{exp}$	S_i/S_{O1s}	$X_{i,O1s}^{exp}$	S_i/S_{O1s}
Y 3d	6.24	1.18	1.76	1087	0.66	2.062	1.000	1.361	1.000	0.247	0.214	0.253	0.306
Ba 4d	5.41	1.33	1.76	1166	0.62	2.062	1.444	1.361	1.055	0.306	0.310	0.249	0.323
Ba $3d_{5/2}$	24.75	1.10	0.82	476	1.52	1.317	1.009	1.062	0.537	0.205	0.216	0.283	0.164
Ba $3d_{3/2}$	17.04	1.10	0.82	460	1.57	1.317	1.009	1.062	0.537	0.216	0.216	0.294	0.164
Cu $2p_{3/2}$	15.87	1.30	0.66	321	2.26	1.205	1.386	1.030	0.777	0.281	0.297	0.062	0.238
O 1s	2.85	2.00	1.35	725	1.00	1.727	4.664	1.215	3.270	1.000	1.000	1.000	1.000

σ, β, λ, E_{kin} and T_{tot} are described in eqs. (1)–(7). The photoelectron take-off angle is denoted by φ. The geometric factor $g_i(\varphi)$ and structural factor $S_i(\varphi)$ are defined in eq. (5). The experimental values $X_{i,O1s}^{exp}$ and theoretical values S_i/S_{O1s} are given in eq. (9). The subscript O 1s indicates that these values have been normalized to the O 1s core level.

ends. In fig. 2, the Y-plane is chosen and for the structural factors $S_i(\varphi)$ we find:

$$S_{Y\,3d}(\varphi) = \exp\left(\frac{-0}{\lambda_{Y\,3d}\cos\varphi}\right) = 1,$$

$$S_{Ba\,4d}(\varphi) = \exp\left(\frac{-3.89}{\lambda_{Ba\,4d}\cos\varphi}\right) + \exp\left(\frac{-7.79}{\lambda_{Ba\,4d}\cos\varphi}\right),$$

$$S_{O\,1s}(\varphi) = 2\exp\left(\frac{-1.95}{\lambda_{O\,1s}\cos\varphi}\right) + \exp\left(\frac{-3.89}{\lambda_{O\,1s}\cos\varphi}\right) + \exp\left(\frac{-5.84}{\lambda_{O\,1s}\cos\varphi}\right) + \exp\left(\frac{-7.75}{\lambda_{O\,1s}\cos\varphi}\right) + 2\exp\left(\frac{-9.73}{\lambda_{O\,1s}\cos\varphi}\right),$$

$$S_{Cu\,2p}(\varphi) = \exp\left(\frac{-1.95}{\lambda_{Cu\,2p}\cos\varphi}\right) + \exp\left(\frac{-5.84}{\lambda_{Cu\,2p}\cos\varphi}\right) + \exp\left(\frac{-9.73}{\lambda_{Cu\,2p}\cos\varphi}\right). \quad (17)$$

$S_{Ba\,3d_{5/2}}(\varphi)$ and $S_{Ba\,3d_{3/2}}(\varphi)$ are calculated analogously to $S_{Ba\,4d}(\varphi)$, by insertion of $\lambda_{Ba\,3d_{5/2}}$ and $\lambda_{Ba\,3d_{3/2}}$, respectively. For 0° and 60° photoelectron take-off angle, $S_i(\varphi)$ values have been calculated and the results are presented in table 2.

Finally, in the last four columns of table 2, the experimental values $X^{exp}_{i,O\,1s}(\varphi)$ as defined by eq. (9), and the ratios $S_i(\varphi)/S_{O\,1s}(\varphi)$ obtained from the theory given in section 2, can be compared. As indicated by the subscript O 1s, these values are given relative to those of O 1s core level. From table 2 a remarkably good agreement between the experimental values and those predicted by theory can be observed, especially for the outlined quantities. The deviations between theory and experiment for the Ba 3d and Cu 2p levels at $\varphi = 60°$ are ascribed to effects of surface roughness, see section 5. To determine the structural factors $S_i(\varphi)$ that describe these measurements optimally, we calculated the residue s. It is defined in eq. (15), where:

$$Y_i = \frac{S_i(\varphi)}{S_{O\,1s}(\varphi)}, \quad Y_i^{exp} = X^{exp}_{i,O\,1s}(\varphi). \quad (18)$$

Using the outlined quantities in table 2, s was calculated as a function of the layer ending the high-T_c superconducting $YBa_2Cu_3O_{7-\delta}$ thin film. In table 3, the values of s are given. We see that the residue s is minimal for a thickness of the surface layer of $d \approx 1.0$ nm and layer 1. The Y layer is indicated as layer 1, the CuO_2 layer as layer 2 and the BaO layer as layer 3, etc., see fig. 2. Since the calculations showed

Table 3
Residue s as function of layer forming the interface between the superconducting $YBa_2Cu_3O_{7-\delta}$ thin film and non-superconducting surface layer

Layer ending the superconducting $YBa_2Cu_3O_{7-\delta}$ film	Residue s
1	0.01
2	0.06
3	0.1
4	0.04
5	0.04
6	0.03

Layer 1 is the Y layer, layer 2 is the CuO_2 layer, layer 3 is the BaO layer, etc., see sections 2 and 4.2.

that the error function s strongly depends on the thickness d, the estimate $d \approx 1.0$ nm is an accurate estimate, as will be confirmed in section 4.3. For the Y layer the residue is minimal, so this atomic layer forms the interface between the superconducting $YBa_2Cu_3O_{7-\delta}$ thin film and the non-superconducting surface layer.

4.3. Composition of the non-superconducting surface layer

The composition of the non-superconducting surface layer differs strongly from the high-T_c superconducting $YBa_2Cu_3O_{7-\delta}$ thin film. Neglecting a possible layered structure of the surface layer and effects of surface roughness, for the elemental photoelectron intensity ratio $R^l_{i,j}$ at 0° photoelectron take-off angle, we may write [1,2,26]:

$$R^l_{i,j} = \frac{\sigma_{i,k} n^l_i \lambda_i \left[1 - \frac{1}{4}\beta_{i,k}(3\cos^2\vartheta_k - 1)\right]\left[1 - \exp(-d/\lambda_i)\right]}{\sigma_{j,l} n^l_j \lambda_j \left[1 - \frac{1}{4}\beta_{j,l}(3\cos^2\vartheta_k - 1)\right]\left[1 - \exp(-d/\lambda_j)\right]}, \tag{19}$$

where n^l_i is the atomic concentration of element i in the surface layer. For the atomic concentration ratios we find, with $d = 1.0$ nm:

$$n^l_Y : n^l_{Ba} : n^l_{Cu} : n^l_O : n^l_C = 0 : 0.2 : 0.1 : 1 : 0.8, \tag{20}$$

so this surface layer consists mainly of compounds containing oxygen and carbon, that is, $BaCO_3$ and C. Only a small volume fraction ($\sim 20\%$) of the layer is formed by Ba- and Cu-oxides. These oxides are probably in the form of $BaCuO_2$ [6], since Cu^{1+} is found in the surface layer, see section 4.1 above.

4.4. Thickness of the non-superconducting surface layer

As we found in section 2.2, the normalized photoelectron intensity $Y^{exp}_{i,k}(\varphi)$ is used in absolute ARXPS measurements. In eq. (14) the thickness d is the only parameter after the structural factors $S_i(\varphi)$ have been obtained from relative ARXPS measurements, see sections 2.1 and 4.2. Data analysis by a LM fit procedure (see section 2.3) gives information about the reliability of the quantitative information obtained in section 4.2. The thickness d and its confidence limits can be calculated.

To do so, we need to determine the function $G(\varphi)$ as defined in eq. (12) and the structural and geometrical factors, $S_i(\varphi)$ and $g_i(\varphi)$, respectively. On a clean amorphous silicon substrate $G(\varphi)$ was measured and the results are given in fig. 5. Experiments to establish the stability of the spectrometer were performed. Points marked with "+" were measured within 10 h. After 24 h the points marked with

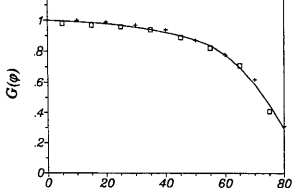

Fig. 5. Measured function $G(\varphi)$, for a description see sections 2.2 and 4.3. Points marked with "+" were measured with 10 h. After 24 h the points marked with "□" were measured with the same instrumental settings. We see that the stability is sufficient. The solid line represents a polynomial fit of the function $G(\varphi)$.

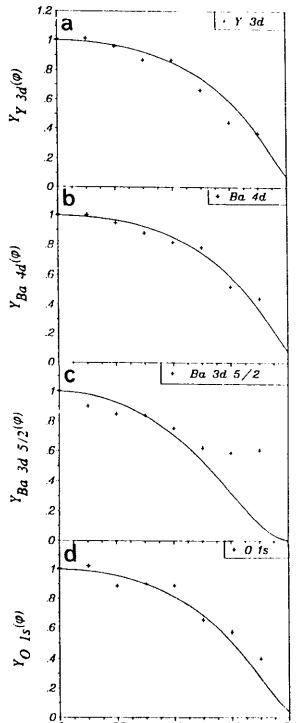

Fig. 6. Absolute ARXPS measurements. The measurements of the Y 3d, Ba 4d and O 1s core levels, indicated with "+", were fitted simultaneously using eq. (14). An optimal thickness of 0.93 nm for the non-superconducting surface layer on the $YBa_2Cu_3O_{7-\delta}$ thin film was found. The result of the fit is given as a solid line, see sections 2.2 and 4.3. Note the deviation between measurements and theoretical curve for the $Ba3d_{5/2}$ level. As discussed in section 5, it is ascribed to the effect of some surface roughness ($O_r \approx 0.6$ nm).

"□" were measured with the same instrumental settings. We see that the stability is sufficient. In fig. 5, the solid line represents a polynomial fit of the function $G(\varphi)$. The structural factors $S_i(\varphi)$ and geometrical factors $g_i(\varphi)$ are obtained from relative ARXPS measurements in section 4.2. With these quantities known, we can calculate the values $Y_{i,k}^{\exp}$ from the intensities of the XPS peaks belonging to elements in the superconducting material, normalized to the intensity at normal take-off. In figs. 6a–6d, $Y_{i,k}^{\exp}(\varphi)$ values are plotted for the Y 3d, Ba 4d, Ba $3d_{5/2}$ and O 1s core levels. The intensities were obtained from simulating the spectra taken at 0°, 10°, ..., 70°. The simulations of the spectra taken at 0° and 60° are given in figs. 4a–4d, as already described in section 4.2. We fitted the values for the Y 3d, Ba 4d and O 1s core levels simultaneously (see section 2.3) using eq. (14) and found for the thickness d and the residue s, as defined in eq. (16):

$$d = 0.93 \pm 0.06 \text{ nm}, \quad \text{residue } s = 0.004. \tag{21}$$

In eq. (14) for the IMFP's λ of the photoelectrons, the values listed in table 2 were used. In fig. 6, the $Y_{i,k}^{\exp}(\varphi)$ are indicated with "+", the result of the fit is given by solid lines. A thickness d with remarkable accuracy has been obtained and it agrees well with the estimate of $d \approx 1.0$ nm, found in section 4.2. These results show that effects of surface roughness must be small. An indication for the surface roughness can be obtained from fig. 6c, the Ba $3d_{5/2}$ level, see the discussion (section 5), below.

4.5. Effects of neglecting the layered structure of the $YBa_2Cu_3O_{7-\delta}$ thin films

If we assume that the elements in the superconducting $YBa_2Cu_3O_{7-\delta}$ thin film are homogeneously distributed, we may write for the elemental photoelectron intensity ratio $R_{i,j}^{\infty}$ at 0° photoelectron take-off angle [1,2], see also eq. (8):

$$R_{i,j}^{\infty} = \frac{\sigma_{i,k} n_i^{\infty} \lambda_i \left[1 - \frac{1}{4}\beta_{i,k}(3\cos^2\vartheta_k - 1)\right] T_{\text{tot}}(E_i) \exp(-d/\lambda_i)}{\sigma_{j,l} n_j^{\infty} \lambda_j \left[1 - \frac{1}{4}\beta_{j,l}(3\cos^2\vartheta_k - 1)\right] T_{\text{tot}}(E_j) \exp(-d/\lambda_j)}. \tag{22}$$

where n_i^{∞} is the atomic concentration of element i in the superconducting material. The film is covered with a non-superconducting surface layer with thickness d. Using the photoelectron intensity ratios determined above, we find for the atomic concentration ratios, with $d = 1.0$ nm:

$$n_Y^{\infty} : n_{Ba}^{\infty} : n_{Cu}^{\infty} : n_O^{\infty} = 1.4 : 1.8 : 2.8 : 7. \tag{23}$$

For σ, λ, β and T_{tot} the values listed in table 2 were used.

5. Discussion

An overview of results of photoemission spectroscopy on high-T_c superconductors was given by Lindberg et al. [3]. A thorough discussion on results on $YBa_2Cu_3O_{7-\delta}$ single crystals, cleaved in the spectrometer prior to analysis, is reported by Fowler et al. [11]. The spectra reported here (see figs. 3a–3g) were obtained on a high-T_c superconducting $YBa_2Cu_3O_{7-\delta}$ thin film, after it had been deposited on an yttria-stabilized ZrO_2 (100) single crystal. They reveal that the superconducting layer is not contaminated, except for some $BaCO_3$ and C due to transport through ambient environment from the deposition chamber to the spectrometer. Comparison of our spectra with those reported in the literature [3,5,6,9–11] reveals that our $YBa_2Cu_3O_{7-\delta}$ thin films are of high quality. Our XPS results may be compared to spectra taken on $YBa_2Cu_3O_{7-\delta}$ single-crystal surfaces. On the spectra features are superposed that are assigned to elements in a thin (thickness ~ 1.0 nm) non-superconducting surface layer, mainly consisting of $BaCO_3$ and C. The surface layer also contains some Ba- and Cu-oxides,

probably in the form of $BaCuO_2$. Comparing these results with earlier experiments [4], we may conclude that the quality of the high-T_c superconducting $YBa_2Cu_3O_{7-\delta}$ thin films on which X-ray photoemission spectra are reported here, has greatly improved and that they show clean and smooth surfaces.

Taking into account the layered structure of the material that is investigated, quantitative analysis of our photoemission spectra yields compositional and structural information about the top layer of $YBa_2Cu_3O_{7-\delta}$ thin films. For the first time, relative ARXPS measurements show that the interface between the superconducting $YBa_2Cu_3O_{7-\delta}$ layer and the non-superconducting surface layer is formed by the Y layer. With absolute ARXPS measurements the thickness of the surface layer can be determined accurately and we find $d = 0.93 \pm 0.06$ nm. The results presented here show a very good agreement between the modelling performed in section 2 and experiments.

It is important to note that in our model we described the $YBa_2Cu_3O_{7-\delta}$ film to be a single crystal. If we do not so and assume that in the superconducting $YBa_2Cu_3O_{7-\delta}$ thin film the elements are homogeneously distributed and that the film is covered with a non-superconducting surface layer, we find: $n_Y^{\wedge} : n_{Ba}^{\wedge} : n_{Cu}^{\wedge} : n_O^{\wedge} = 1.4 : 1.8 : 2.8 : 7$ (see section 4.5), for the Y concentration an error of 40%. In our model the strongest deviation between theory and experiment arises for the Y 3d core level, with a relative error of 15%, as can be seen in table 2 for $\varphi = 0°$. This large improvement in agreement with theoretical and experimental values can be easily understood with our finding that the material has a layered structure with different composition. In the high-T_c superconducting $YBa_2Cu_3O_{7-\delta}$ film the first Y layer partly shields the photoelectrons of the elements Ba, Cu and O below it. The results show that in the qualitative analysis of XPS spectra, the effect of a layered structure of the investigated material may not be neglected.

For σ, β and λ values were taken from the literature. Especially in the case of λ, discrepancies on the order of 10% must be expected between theoretical and experimental values [27]. However, using the theoretical values, a very good agreement between model and experiment has been shown in this report. Therefore, the values as tabulated in table 2 may be considered to describe the actual experimental values fairly well.

If we look at the simulations of the Y 3d level, shown in fig. 4a, a small high BE tail can be seen. Since the intensity of this tail does not depend strongly on photoelectron take-off angle, as the high BE features in the Ba- and O-spectra do, no attempt to simulate this tail was made. The choice of the starting- and end-point for the Shirley background subtraction procedure [33] may affect its intensity. A different choice may decrease the intensity at high BE and give even a better agreement of the theoretical and experimental values in table 2. The high BE tail may also be due to some imperfections in the $YBa_2Cu_3O_{7-\delta}$ thin film together with some surface roughness.

In the modelling of the high-T_c superconducting $YBa_2Cu_3O_{7-\delta}$ thin film as described in section 2, the layers were assumed to be homogeneous with a uniform thickness. Since the film thickness was 10 nm and XPS peaks of the YSZ substrate could not be observed, pin-holes in the $YBa_2Cu_3O_{7-\delta}$ layer can be excluded. Secondary electron microscopy (SEM) studies revealed no surface roughness, for focussing some dust particles present on the film surface had to be used. Absolute ARXPS measurements are sensitive to surface roughness, as can be seen in figs. 6a–6d. For large IMFP λ of the photoelectrons, that is for the Y 3d, Ba 4d and O 1s core levels with $\lambda = 1.76$, 1.76 and 1.35 nm, respectively, the values predicted by our model and the experimental values agree well. For small λ of the $Ba\,3d_{5/2}$ level, where $\lambda = 0.82$ nm, effects of surface roughness become observable at large photoelectron take-off angles φ, with $\varphi > 45°$, see fig. 4c. The $Ba\,3d_{3/2}$ level showed the same behaviour. From these results a rough estimate of the surface roughness O_r can be obtained. We may approximate O_r by $\lambda \cos \varphi_r$, with φ_r the photoelectron take-off angle at which measurements and theory start to deviate by more than 10%. For the $Ba\,3d_{5/2}$ level we find $O_r \approx 0.6$ nm.

6. Conclusions

By means of a modified RF-magnetron sputtering technique, high-T_c superconducting $YBa_2Cu_3O_{7-\delta}$ thin films with a transition temperature $T_{c,zero}$ of about 90 K were obtained routinely for film thicknesses of 8–300 nm. The critical current density j_c at 77 K of these films is found to be higher than 1×10^6 A/cm^2. The films are perfectly c-axis oriented.

X-ray photoemission spectra acquired on our high-T_c superconducting $YBa_2Cu_3O_{7-\delta}$ thin films resemble spectra taken on $YBa_2Cu_3O_{7-\delta}$ single crystals, cleaved in situ in the XPS spectrometer. On the spectra features are superposed that are assigned to a thin (thickness ~ 1.0 nm) non-superconducting surface layer.

A good agreement between theory and experiment was found in this investigation. Including the effect of the layered structure of c-axis oriented $YBa_2Cu_3O_{7-\delta}$ thin films in a model for quantitative analysis of photoemission spectra, relative ARXPS measurements provide structural and chemical information about the top layer of an $YBa_2Cu_3O_{7-\delta}$ thin film. With absolute ARXPS measurements the thickness of a non-superconducting thin surface layer can be determined very accurately. For the first time, relative ARXPS measurements show that electronically the interface between the superconducting $YBa_2Cu_3O_{7-\delta}$ film and the surface layer is formed by the atomic Y layer. The surface layer consists mainly of $BaCO_3$ and C. A small volume fraction (~ 20%) contains Ba- and Cu-oxides, probably in the form of $BaCuO_2$. From absolute ARXPS measurements, the thickness of the surface layer was calculated to be 0.93 ± 0.06 nm. The surface roughness of the $YBa_2Cu_3O_{7-\delta}$ films is on the order of 0.6 nm. For large IMFP λ of the photoelectrons, effects of surface roughness on the photoelectron intensities may be neglected.

If we neglect the layered structure of the $YBa_2Cu_3O_{7-\delta}$ thin films and assume that in the film the elements are homogeneously distributed and that the film is covered with a non-superconducting surface layer, we find: $n_Y^\infty : n_{Ba}^\infty : n_{Cu}^\infty : n_O^\infty = 1.4 : 1.8 : 2.8 : 7$. For the Y concentration this is an error of 40%. In the model we developed here the strongest deviation between theory and experiment decreases to an error of 15%, which may be considered a large improvement in the understanding of ARXPS experiments on c-axis oriented high-T_c superconducting $YBa_2Cu_3O_{7-\delta}$ thin films. The results presented here show that the layered structure of materials that are investigated, is essential to the quantitative analysis of X-ray photoemission spectra, taken on these materials.

Acknowledgements

This work is part of the research program of the "Stichting voor Fundamenteel Onderzoek der Materie (FOM)", which is financially supported by the "Nederlandse organisatie voor Wetenschappelijk Onderzoek (NWO)", and was made possible by support of the "Centrum voor Materialen Onderzoek (CMO)", Enschede. The authors would like to thank J. Halbritter for stimulating discussions.

References

[1] M. Cardona and L. Ley, Eds., Photoemission in Solids I (Springer, New York, 1978).
[2] D. Briggs and M.P. Seah, Eds., Practical Surface Analysis by Auger and X-ray Photoelectron Spectroscopy (Wiley, Chichester, 1983).
[3] P.A.P. Lindberg, Z.-X. Chen, W.E. Spicer and I. Lindau, Surf. Sci. Rep. 11 (1990) 1.
[4] J. Halbritter, P. Walk, H.-J. Mathes, B. Häuser and H. Rogalla, Z. Phys. B 73 (1988) 277.
[5] X.D. Wu, A. Inam, M.S. Hegde, T. Venkatesan, C.C. Chang, E.W. Chase, B. Wilkens and J.M. Tarascon, Phys. Rev. B 38 (1988) 9307.

[6] C.C. Chang, M.S. Hegde, X.D. Wu, B. Dutta, A. Inam, T. Venkatesan, B.J. Wilkens and J.B. Wachtman, Jr., J. Appl. Phys. 67 (1990) 7483.
[7] P.A.P. Lindberg, I. Lindau and W.E. Spicer, Phys. Rev. B 40 (1989) 6822.
[8] W.A.M. Aarnink, J. Gao, H. Rogalla and A. van Silfhout, J. Less-Common Met. 164/165 (1990) 321.
[9] H.M. Meyer, D.M. Hill, T.J. Wagener, Y. Gao, J.H. Weaver, D.W. Capone and K.C. Goretta, Phys. Rev. B 38 (1988) 6500.
[10] S.L.T. Andersson and J.C. Otamiri, Appl. Surf. Sci. 45 (1990) 1.
[11] D.E. Fowler, C.R. Brundle, J. Lerczak and F. Holtzberg, J. Electron Spectrosc. 52 (1990) 323.
[12] D. van der Marel, J. van Elp, G.A. Sawatzky and D. Heitmann, Phys. Rev. B 37 (1988) 5136.
[13] J. Ghijsen, L.H. Tjeng, J. van Elp, H. Eskes, J. Westerink, G.A. Sawatzky and M.T. Czyzyk, Phys. Rev. B 38 (1988) 11322.
[14] G. Frank, Ch. Ziegler and W. Göpel, Phys. Rev. B 43 (1991) 2828.
[15] W.A.M. Aarnink, J. Gao, H. Rogalla and A. van Silfhout, in: Proc. Symp. A1, Int. Conf. on Advanced Materials (ICAM 1991), Strasbourg, France, 27–31 May 1991, to be published.
[16] J. Gao, B. Häuser and H. Rogalla, J. Appl. Phys. 67 (1990) 2512.
[17] J. Gao, W.A.M. Aarnink, G.J. Gerritsma and H. Rogalla, Appl. Surf. Sci. 46 (1990) 74.
[18] J. Gao, W.A.M. Aarnink, G.J. Gerritsma and H. Rogalla, Physica C 177 (1991) 384.
[19] J. Gao, W.A.M. Aarnink, G.J. Gerritsma and H. Rogalla, Physica C 171 (1990) 126.
[20] J. Gao, W.A.M. Aarnink, G.J. Gerritsma, D. Veldhuis and H. Rogalla, in: Proc. 1990, IEEE Trans. Magn. 27 (1981) 3062.
[21] W.A.M. Aarnink, A. Weishaupt and A. van Silfhout, Appl. Surf. Sci. 45 (1990) 37.
[22] S. Tougaard, J. Vac. Sci. Technol. A 5 (1987) 1230.
[23] S. Tougaard and P. Sigmund, Phys. Rev. B 25 (1982) 4452.
[24] B.C. Henke, Phys. Rev. B 6 (1972) 94.
[25] J.H. Scofield, J. Electron Spectrosc. 8 (1976) 129.
[26] R.F. Reilmann, A. Msezane and S.T. Manson, J. Electron Spectrosc. 8 (1976) 389.
[27] M.P. Seah and W. Dench, Surf. Interf. Anal. 1 (1979) 2.
[28] D.W. Marquardt, J. Soc. Indust. Appl. Math. 11 (1963) 431.
[29] S.Y. Kim and K. Vedam, Appl. Opt. 25 (1986) 2013.
[30] XSAM800 Operators Handbook, Kratos Analytical Instruments.
[31] See ref. [2], p. 431.
[32] DS 800 Users Guide, Kratos Analytical Instruments.
[33] D.A. Shirley, Phys. Rev. B 5 (1972) 4709.
[34] P. Steiner, V. Kinsinger, I. Sander, B. Siegwart, S. Hüfner, C. Politis, R. Hoppe and H.P. Müller, Z. Phys. B 67 (1987) 497.
[35] J.D. Jorgensen, B.W. Veal, A.P. Paulikas, L.J. Nowicki, G.W. Crabtree, H. Claus and W.K. Kwok, Phys. Rev. B 41 (1990) 1863.
[36] W.H. Gries, J. Vac. Sci. Technol. A 7 (1989) 1655.